


# Paclitaxel and Erlotinib-co-loaded Solid Lipid Core Nanocapsules: Assessment of Physicochemical Characteristics and Cytotoxicity in Non-small Cell Lung Cancer

Biki Gupta<sup>1</sup> · Bijay Kumar Poudel<sup>1</sup> · Shobha Regmi<sup>1</sup> · Shiva Pathak<sup>1</sup> · Hima Bindu Ruttala<sup>1</sup> · Milan Gautam<sup>1</sup> · Gyeong Jin An<sup>1</sup> · Jee-Heon Jeong<sup>1</sup> · Han-Gon Choi<sup>2</sup> · Chul Soon Yong<sup>1</sup> · Jong Oh Kim<sup>1</sup> 

Received: 20 September 2017 / Accepted: 20 December 2017 / Published online: 13 March 2018  
© Springer Science+Business Media, LLC, part of Springer Nature 2018

## ABSTRACT

**Purpose** Lung cancer is the leading cause of cancer-related deaths. The aim of this study was to design solid lipid core nanocapsules (SLCN) comprising a solid lipid core and a PEGylated polymeric corona for paclitaxel (PTX) and erlotinib (ERL) co-delivery to non-small cell lung cancer (NSCLC), and evaluate their physicochemical characteristics and *in vitro* activity in NCI-H23 cells.

**Methods** PTX/ERL-SLCN were prepared by nanoprecipitation and sonication and physicochemically characterized by dynamic light scattering, transmission electron microscopy, differential scanning calorimetry, X-ray diffraction, and Fourier-transform infrared spectroscopy. *In vitro* release profiles at pH 7.4 and pH 5.0 were studied and analyzed. *In vitro* cytotoxicity and cellular uptake and apoptosis assays were performed in NCI-H23 cells.

**Results** PTX/ERL-SLCN exhibited appropriately-sized spherical particles with a high payload. Both PTX and ERL showed pH-dependent and sustained release *in vitro* profiles. PTX/ERL-SLCN demonstrated concentration- and time-dependent uptake by NCI-H23 cells and caused dose-dependent cytotoxicity in the cells, which was remarkably greater than that of not only the free individual drugs but also

the free drug cocktail. Moreover, well-defined early and late apoptosis were observed with clearly visible signs of apoptotic nuclei.

**Conclusion** PTX/ERL-SLCN could be employed as an optimal approach for combination chemotherapy of NSCLC.

**KEY WORDS** Erlotinib · paclitaxel · solid lipid core nanocapsules · non-small cell lung cancer

## ABBREVIATIONS

ABS	Acetate buffer solution
DDAB	Didodecyldimethylammonium bromide
DLS	Dynamic light scattering
DMEM	Dulbecco's Modified Eagle's medium
DMSO	Dimethyl sulfoxide
DSC	Differential scanning calorimetry
EGFR	Epidermal growth factor receptor
ERL	Erlotinib
FACS	Fluorescence-activated cell sorting
FBS	Fetal bovine serum
FTIR	Fourier-transform infrared spectroscopy
GMS	Glyceryl monostearate
HPLC	High-performance liquid chromatography
LC	Loading capacity
LE	Loading efficiency
MTT	3-(4,5-dimethylthiazol-2-yl)-2,5-diphenyltetrazolium bromide
MWCO	Molecular weight cut-off
NSCLC	Non-small cell lung cancer
PBS	Phosphate-buffered saline
PDI	Polydispersity index
PEG	Poly(ethylene glycol)
PTX	Paclitaxel
SCLC	Small cell lung cancer
SL	Soya lecithin
SLCN	Solid lipid core nanocapsules

**Electronic supplementary material** The online version of this article (<https://doi.org/10.1007/s11095-017-2337-6>) contains supplementary material, which is available to authorized users.

✉ Chul Soon Yong  
csyong@yu.ac.kr

✉ Jong Oh Kim  
jongohkim@yu.ac.kr

<sup>1</sup> College of Pharmacy, Yeungnam University  
214-1, Dae-Dong, Gyeongsan 712-749, South Korea

<sup>2</sup> College of Pharmacy, Institute of Pharmaceutical Science and Technology, Hanyang University, 55, Hanyangdaehak-ro Sangnok-gu, Ansan 426-791, South Korea

TEM	Transmission electron microscopy
TKI	Tyrosine kinase inhibitor
XRD	X-ray diffraction

## INTRODUCTION

Lung cancer is the most common cause of cancer-related death worldwide in men, and the second in women, only behind breast cancer. In the developed countries, however, it is the most common cause of cancer-related death even in women (1). Non-small cell lung cancer (NSCLC) is one of the two main types of lung cancer, the other being small cell lung cancer (SCLC), and accounts for nearly 85% of all of the lung cancer cases (2). The standard treatment strategy of NSCLC includes surgery in tandem with adjuvant chemotherapy, with or without radiotherapy, depending on the disease stage and characteristics (3). The chemotherapeutic agents that have been reported to exhibit varying degrees of therapeutic success at different stages of NSCLC include cisplatin, gemcitabine, paclitaxel, docetaxel, irinotecan, erlotinib, pemetrexed, vinblastine, vinorelbine, etoposide, and mitomycin C among others, either as single agents or in various combinations (4–25). As compared with single-agent therapy, combination therapy in NSCLC has been reported to be considerably efficacious with higher response rates and longer time to progression (26,27).

Paclitaxel (PTX) is a cytotoxic agent that binds to the  $\beta$ -tubulin subunit of the microtubules and thereby interrupts mitotic spindle formation, causing mitotic arrest at the G2/M interphase of the cell cycle. It has been widely used as the first-line therapy for advanced NSCLC both as a single-agent and in combination with other cytotoxic agents. While combinations of PTX with platinum-based agents have been widely used, severe toxicity associated with such combinations has largely discouraged their use. Recently, molecular-targeted agents have demonstrated synergistic therapeutic advantages in combination with PTX, and therefore have been evaluated as adjuvants in early NSCLC (28,29). Erlotinib (ERL) is an epidermal growth factor receptor tyrosine kinase inhibitor (EGFR-TKI) that improved median survival, quality of life, and related symptoms in advanced and metastatic NSCLC (30). Combination of ERL with chemotherapeutic agents has been suggested as a viable option for the treatment of NSCLC, especially in EGFR mutation-positive cases (31). ERL and PTX or carboplatin combinations in an intercalated regimen have been reported to show high progression-free survival rate in NSCLC patients with activating-EGFR mutations (32).

Nanoparticle drug delivery systems, ever since their emergence, have revolutionized the field of drug delivery for cancer therapy. For combination chemotherapy, these nanoparticle systems can provide additional advantages of improved

efficacy and safety. These systems offer the capability to control or modify the drug release behavior, which can be utilized to optimize the pharmacokinetics, biodistribution, and stability of the chemically as well as pharmacologically disparate drugs (33,34). Nanoparticles are innately capable of long plasma circulation, which can be further enhanced by surface modification with hydrophilic polymers such as polyethylene glycol (PEG). Additionally, further appropriate modifications can be employed to engineer stimuli-responsive or targeted carrier systems (35). Thus, nanotechnology can provide long-circulating, specifically-targeted systems that are responsive to the tumor microenvironment and capable of controlled release of combination chemotherapeutic drugs at fixed ratios or independently tuned rates, which is not possible with free drug combinations.

Various nanoscale architectures have been employed for chemotherapeutic delivery over the years, including polymer-derived systems and lipid-based systems such as liposomes, with mixed results. Liposomes, for instance, have been reported to offer innumerable advantages to tumor delivery of chemotherapeutic agents. However, major limitations related with stability and scale-up of liposomes have restricted their clinical application (36,37). On the other hand, polymeric nanoparticles, despite exhibiting high stability, are not as biocompatible as lipid-based nanoparticles and often exhibit low degree of encapsulation of therapeutic agents (38). Hence, recently the focus has shifted towards hybrid systems, comprising of both lipid and polymeric components, with the aim to combine the advantages of both the system while overcoming their individual limitations (39). In the present study, we have attempted to assemble solid lipid core nanocapsules (SLCNs) for co-delivery of PTX and ERL as chemotherapeutic combination. These PTX- and ERL-co-loaded SLCN (PTX/ERL-SLCNs) consist of solid lipid cores, which accommodate both PTX and ERL, and block copolymer coronae with PEGylated exterior.

## MATERIALS AND METHODS

### Materials

Paclitaxel (PTX) was acquired from Shaanxi Top Pharm Chemical Co. Ltd. (Xi'an, China), and Erlotinib (ERL) from LC Laboratories (Woburn, MA, USA). Glycerol monostearate (GMS) was procured from Tokyo Chemical Industry Co. Ltd. (Tokyo, Japan), soya lecithin (SL) from Junsei Chemical Co. Ltd. (Tokyo, Japan), poloxamer 188 (PX188) from BASF (Ludwigshafen, Germany), mPEG<sub>1K</sub>-*b*-PLD<sub>10</sub> (methoxy-poly(ethylene glycol)-*block*-poly(L-aspartic acid sodium salt, mPEG-*b*-pAsp) from Alamanda Polymers (Huntsville, AL, USA), and Didodecyldimethylammonium

bromide (DDAB) and coumarin 6 from Sigma-Aldrich (St Louis, Missouri, USA).

### Preparation of Solid Lipid Core Nanocapsules

PTX/ERL-SLCNs were prepared by a two-step process comprising nanoprecipitation and sonication. Briefly, GMS (60 mg) was melted at 55°C, mixed with SL (15 mg) and DDAB (5 mg), and dissolved in methanol (2 ml). PTX and ERL (5 mg each) were then added to this methanolic solution, cooled, and stirred to dissolve. To an aqueous solution of PX188 (50 mg in 10 ml), the above solution was added using a 3-ml syringe over 5 min while stirring at 1000 rpm, followed by an additional 10-min stirring. The resulting solid lipid nanoparticles were washed in a dialysis bag (MWCO = 3.5 kDa) against distilled water for 24 h. Lastly, 1 ml of 12 mg/ml mPEG-*b*-pAsp was added to the above aqueous dispersion of solid lipid nanoparticles and the mixture was subjected to moderate sonication for 30 min, followed by undisturbed standing overnight. This resulted in formation of PTX/ERL-SLCN, with a solid lipid core containing PTX and ERL as anticancer agents, and a polymeric encapsulating shell having PEGylated exterior. For blank solid lipid nanocapsules (SLCN), the above procedure was repeated without the addition of the drugs, whereas for coumarin 6-loaded SLCN (Cou-SLCN), the chemotherapeutic drugs were replaced with coumarin 6.

### Particle Size and $\zeta$ -Potential Characterization

Dynamic light scattering (DLS) technique was used to estimate the hydrodynamic particle size and the  $\zeta$ -potential of PTX/ERL-SLCN. For DLS measurements, PTX/ERL-SLCN, sufficiently diluted in distilled water, was taken in a cuvette and placed inside a Nano-S90 ZetaSizer (Malvern Instruments, UK). The ZetaSizer, equilibrated at a temperature of 25°C, measured the DLS characteristics of the nanoparticles at a scattering angle of 92°. All the measurements were carried out in triplicates.

### Drug Loading and Loading Efficiency

The loading capacity (LC) and loading efficiency (LE) of PTX and ERL in PTX/ERL-SLCN were determined based on following equations:

$$LC = W_D / (W_C + W_D) \times 100$$

$$LE = W_D / W_{D_0} \times 100$$

Where  $W_D$ ,  $W_C$ , and  $W_{D_0}$  represent weight of the drug loaded in the carrier, weight of the carrier, and weight of the initial drug input, respectively. The weight of PTX and ERL loaded in the carrier was determined using HPLC. Agilent 1260

Infinity HPLC set-up was used with Inertsil ODS-3 column (5  $\mu$ m, 4.6  $\times$  150 mm). Same mobile phase consisting of acetonitrile and 20 mM aqueous monopotassium phosphate solution (52.5:47.5 *v/v*) was used for both drugs. It was maintained at a flow rate of 1 ml/min and a column temperature of 25  $\pm$  0.5°C. Aliquots (20  $\mu$ L) of the samples were injected into the column and the detection was made at a wavelength of 227 nm for both drugs.

### Transmission Electron Microscopy

The morphological features of PTX/ERL-SLCN were studied by transmission electron microscopy (TEM). The nanoparticles were stained with 2% *w/v* phototungstic acid and then placed over a carbon film-coated copper grid. The grid was placed under an infrared lamp to allow the sample to dry. The TEM images were captured using an H7600 transmission electron microscope.

### Physical State Characterization

#### Differential Scanning Calorimetry

Differential scanning calorimetry (DSC) was performed by using a DSC-Q200 differential scanning calorimeter (TA Instruments, USA) on freeze-dried PTX/ERL-SLCN, freeze-dried blank SLCN, and free powdered drugs (PTX & ERL). Weighed amounts of the samples were taken in hermetic aluminum sample pans, and the pans were sealed and placed inside the calorimeter. The samples were then heated at the rate of 20°C/min over a range of 40 to 240°C in a dynamic nitrogen atmosphere.

#### X-Ray Diffraction

X-ray diffraction (XRD) characterization of freeze-dried PTX/ERL-SLCN, freeze-dried blank SLCN, and the free powdered drugs was performed by using a vertical goniometer and X-ray diffractometer (X'pert PRO MPD diffractometer, The Netherlands). Ni-filtered CuK $\alpha$ -radiation scattered in the crystalline regions of the samples were recorded at room temperature over a diffraction angle ( $2\theta$ ) range of 10° to 60° at a scanning rate of 5°/min, a voltage of 40 kV, and a current of 30 mA.

#### Fourier-Transform Infrared Spectroscopy

Fourier-transform infrared (FTIR) spectra of freeze-dried PTX/ERL-SLCN, freeze-dried blank SLCN, and free powdered drugs were recorded by using Nicolet Nexus 670 FTIR Spectrometer (Thermo Fisher Scientific Inc., Waltham, MA, USA). The spectra were recorded by using attenuated total

reflectance (ATR) method over a wavelength range of 550 to 4000  $\text{cm}^{-1}$  and at a resolution of 16.

### **In Vitro Drug Release Study**

The *in vitro* release patterns of PTX and ERL from PTX/ERL-SLCN at pH 7.4 and pH 5.0 were studied by diffusion method. Briefly, 2 ml of PTX/ERL-SLCN was taken in a dialysis bag, which was clipped at both ends and kept in a 50 ml centrifuge tube containing 25 ml of phosphate buffered saline (PBS, pH 7.4) or acetate buffer solution (ABS, pH 5.0). For analysis of PTX and ERL, 0.5 ml of the release medium was withdrawn at fixed intervals, which was replaced each time with an equal volume of fresh medium. The amounts of PTX and ERL contained in each of the samples were determined by HPLC analysis, as discussed above. Statistical evaluation of the drug release kinetics was performed by using KinetDS software whereby the resulting release equations were fitted to a number of release model equations and the regression coefficient and rate constant in each case was determined.

### **In Vitro Cytotoxicity Assay**

MTT assays were performed on NCI-H23 human lung adenocarcinoma (non-small cell lung cancer) cell lines. Firstly, PTX, ERL, and PTX and ERL in various molar combinations in PTX/ERL-SLCN (5:1, 2:1, 1:1, 1:2, 1:5) were used to determine the optimum molar ratio for combining PTX and ERL in PTX/ERL-SLCN, based on the  $\text{IC}_{50}$  of combination, to obtain maximum inhibition of the cancer cells. Thereafter, MTT assay was conducted using PTX/ERL-SLCN containing PTX and ERL in the optimized molar ratio; free PTX, free ERL, and PTX/ERL cocktail combined in the above optimized ratio were used to investigate their inhibitory potential on the proliferation of NCI-H23 cells. Briefly,  $1 \times 10^4$  cells, suspended in high glucose DMEM supplemented with 10% FBS, were seeded in each well of a 96-well plate. The plates were incubated overnight at 37°C to allow the cells to adhere to the well surfaces. Then, the growth medium was replaced with various dilutions of PTX, ERL, PTX/ERL, and PTX/ERL-SLCN solutions prepared in growth media. The plates were again incubated at 37°C for 48 h, following which the drug-containing media were removed. Subsequently, the wells were washed with PBS and 100  $\mu\text{L}$  aliquots of 1.25 mg/ml MTT in serum-free DMEM were added to each well. After 3-h incubation at 37°C, 100  $\mu\text{L}$  DMSO was added to each well, and the number of viable cells was ascertained by measuring the absorbance at 570 nm on a microplate reader (Multiskan EX, Thermo Scientific). The absorbance values were utilized to calculate the

cell viability using the following formula: cell viability =  $(A_{\text{sample}} / A_{\text{control}}) \times 100\%$ , where A represents absorbance at 570 nm.

### **Cellular Uptake Analysis**

#### **FACS Analysis**

Fluorescence-activated cell sorting (FACS) analysis was used to study the cellular uptake of SLCN in NCI-H23 cells. The cells ( $2 \times 10^5$ /well) were seeded in a 6-well plate, incubated overnight at 37°C, and treated with Cou-SLCN by varying the drug concentration and incubation time to determine the concentration- and time-dependence of cellular uptake, followed by incubation at 37°C. Thereafter, the cells were washed twice with PBS, detached from the well surfaces, and re-dispersed in 1 ml of PBS. The cells were then immediately subjected to FACS analysis by using FACS Verse (BD Biosciences, CA, USA). Untreated cells were used as internal control.

#### **Fluorescence Microscopy**

For fluorescence microscopy, the cells ( $2 \times 10^5$ ) were seeded in a 12-well plate, incubated overnight at 37°C, treated with Cou-SLCN at various drug concentrations and incubation times. Subsequently, all wells were washed twice with PBS. The cells were then observed under an inverted fluorescence microscope (Nikon Eclipse Ti, Nikon, Japan), and images were captured and analyzed by using NIS-Elements BR 4.20.00 microscope imaging software (Nikon, Japan).

#### **Apoptosis Assay**

FITC-annexin V/ propidium iodide (PI) apoptosis kit (BD Biosciences, San Jose, CA) was used to study the apoptosis of NCI-H23 cells after treatment with PTX/ERL-SLCN. Briefly,  $3 \times 10^5$  cells per well were seeded in a 6-well plate and incubated overnight at 37°C. The cells were treated with PTX, ERL, PTX/ERL, and PTX/ERL-SLCN (with drug concentration equivalent to 2  $\mu\text{g}/\text{ml}$ ). After 24-h incubation at 37°C, the cells were washed twice with cold PBS, detached from the well surfaces, and dispersed in 90  $\mu\text{L}$  of 1X annexin V binding buffer. FITC-annexin and PI (2.5  $\mu\text{L}$  each) were added, and the cells were incubated at room temperature in the dark for 15 min. Finally, 900  $\mu\text{L}$  of 1X annexin V binding buffer was added and the cell samples were analyzed on a BD FACS Verse Flow Cytometer (BD Biosciences, San Jose, CA, USA). Untreated cells were used as an internal control. At least 10,000 events were acquired and analyzed per sample.

## Hoechst Imaging Assay

Hoechst imaging assay was performed to determine any signs or morphological changes in NCI-H23 cells while undergoing apoptosis. Cells ( $3 \times 10^5$  per well) were seeded in a 6-well plate and incubated at 37°C overnight to ensure adherence of the cells to the well surface. Thereafter, the growth media were removed and the cells were treated with adequate dilutions of PTX, ERL, PTX/ERL, and PTX/ERL-SLCN in fresh media. After 24-h incubation, the media were discarded and the cells were washed twice with PBS. Hoechst 33,342 (Sigma-Aldrich) staining solution (2 ml; 2.5 µg/ml) was added to each well and the plate was incubated in the dark at room temperature for 10 min. Finally, the staining solution was removed, the cells were washed with PBS, and images were taken using a fluorescence microscope.

## RESULTS AND DISCUSSION

### Preparation of PTX/ERL-SLCN

PTX/ERL-SLCN consisted of a cationic solid lipid core, co-loaded PTX and ERL as combination chemotherapeutic agents, and a polymeric corona composed of PEG-pAsp. The cationic solid lipid nucleus was fabricated by a 2-step process comprising nanoprecipitation and sonication. Then, a polyanionic mPEG-*b*-pAsp layer was coated over the cationic solid lipid nucleus by electrostatic interaction, resulting in the formation of PTX/ERL-SLCN. The particle size and polydispersity index (PDI) of the cationic nuclei were largely affected by four variables, namely, organic/aqueous phase volume ratio, weight percentage of the drugs (relative to the weight of the carrier), percentage of DDAB, and percentage of Poloxamer 188 (relative to the aqueous phase), which were in accordance with previous reports (40,41). The changes in particle size and PDI in response to changes in these four variables are illustrated in Fig. S1. The  $\zeta$ -potential of the cationic nuclei varied primarily in response to changes in percentage of DDAB, and percentage of Poloxamer 188, as shown in Fig.

S2. The encapsulation efficiency of the drugs was dependent on organic/aqueous phase volume ratio, weight percentage of the drugs, percentage of DDAB, and percentage of Poloxamer 188, as shown in Fig. S3. Correlations between encapsulated drug and the above specified factors were consistent with those reported in previous studies (42,43). The optimized cationic nuclei exhibited a particle size of  $121.0 \pm 1.4$  nm, with a PDI of  $0.193 \pm 0.022$ , and  $\zeta$ -potential of  $44.6 \pm 0.3$  mV. The loading efficiencies of PTX and ERL were  $92.9 \pm 1.1\%$  w/w and  $90.3 \pm 1.3\%$  w/w, respectively for 10% w/w total initial drug input relative to the carrier weight; the corresponding loading capacities were  $4.4 \pm 0.1\%$  w/w and  $4.3 \pm 0.1\%$  w/w, respectively. The coating of the PEG-pAsp polyanionic layer over the cationic solid lipid nucleus was confirmed by the subsequent reversal of  $\zeta$ -potential from cationic to anionic with increasing amount of mPEG-*b*-pAsp (44), as shown in Fig. S4. The schematic representation of PTX/ERL-SLCN formulation is shown in Fig. 1.

### Characterization of PTX/ERL-SLCN

DLS characterization of PTX/ERL-SLCN exhibited a hydrodynamic size of  $195.9 \pm 3.2$  nm, with a PDI of  $0.215 \pm 0.025$ , and a  $\zeta$ -potential of  $-29.8 \pm 0.4$  mV. TEM images revealed spherical particles having dense core and distinctly fainter corona, with particle sizes identical to those observed in DLS characterization (Fig. 2a). These nano-size ranges of PTX/ERL-SLCN are considered suitable to preferentially accumulate into the tumors by enhanced permeability and retention (EPR) effect (45,46). DSC thermograms of the free powdered drugs (PTX and ERL) featured endothermic peaks corresponding to their respective melting points, which were absent in case of PTX/ERL-SLCN as well as in SLCN (Fig. 2b). Similarly, XRD scans of PTX and ERL featured sharp crystalline peaks, while those of PTX/ERL-SLCN, as well as SLCN, featured smooth peaks (Fig. 2c). Together, these results indicated that both the drugs were well encapsulated within the nanoparticle matrix in amorphous or molecularly dispersed state. FTIR spectra of PTX/ERL-SLCN showed that all major peaks of the free powdered drugs were

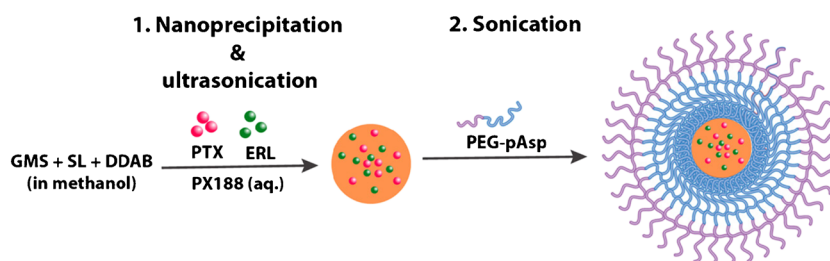
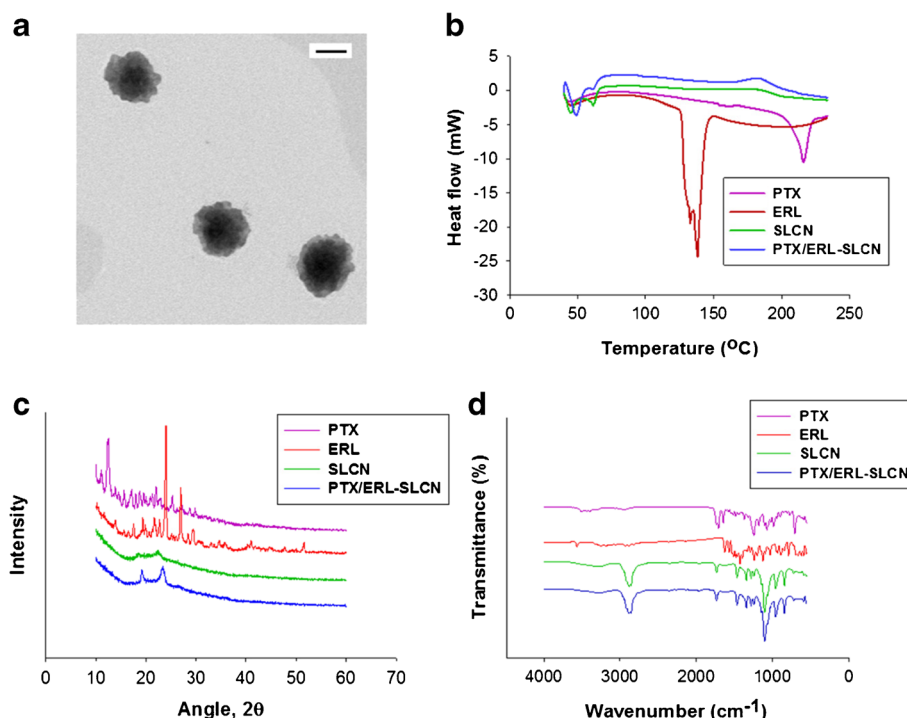


**Fig. 1** Schematic of paclitaxel- and erlotinib-co-loaded solid lipid core nanocapsules (PTX/ERL-SLCN). GMS, glyceryl monostearate; SL, soya lecithin; DDAB, didodecyldimethylammonium bromide; PTX, paclitaxel; ERL, erlotinib; PX188, Poloxamer 188; PEG-pAsp, methoxy poly(ethylene glycol)-block-poly(aspartic acid).

**Fig. 2** Physicochemical characterization of paclitaxel and erlotinib co-loaded solid lipid core nanocapsules (PTX/ERL-SLCN): (a) Transmission electron microscopic (TEM) images of PTX/ERL-SLCN; (b) Differential scanning calorimetry (DSC) thermograms; (c) X-ray diffraction (XRD) diffractograms; and (d) Fourier transform infrared (FTIR) spectra of free PTX, free ERL, blank solid lipid core nanocapsules (SLCN), and PTX/ERL-SLCN. The scale bar = 100 nm.



conserved and no extra peaks were observed (Fig. 2d), ruling out chemical changes to the bound drugs as a result of drug and carrier interactions.

### Drug Release Characteristics

PTX and ERL showed sustained and pH-dependent *in vitro* release from PTX/ERL-SLCN (Fig. 3). The release of both PTX and ERL remarkably increased under acidic conditions (pH 5.0) as compared to that under normal physiologic pH conditions (pH 7.4). The cumulative drug release at 48 h for

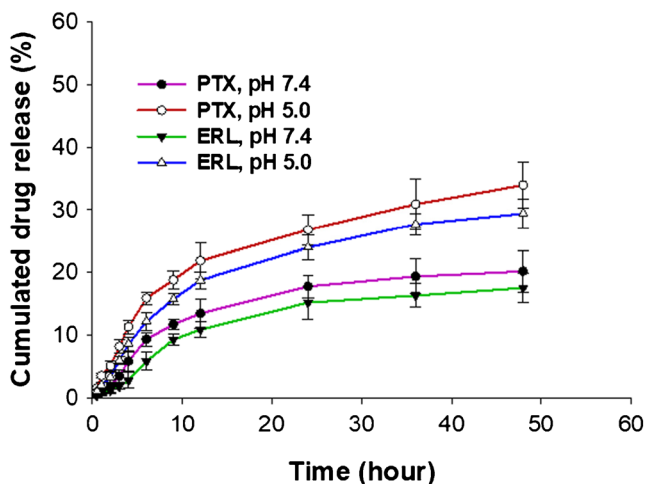


**Fig. 3** *In vitro* release profiles of PTX and ERL from PTX/ERL-SLCN at normal physiologic pH (7.4) and tumoral pH (5.0) conditions.

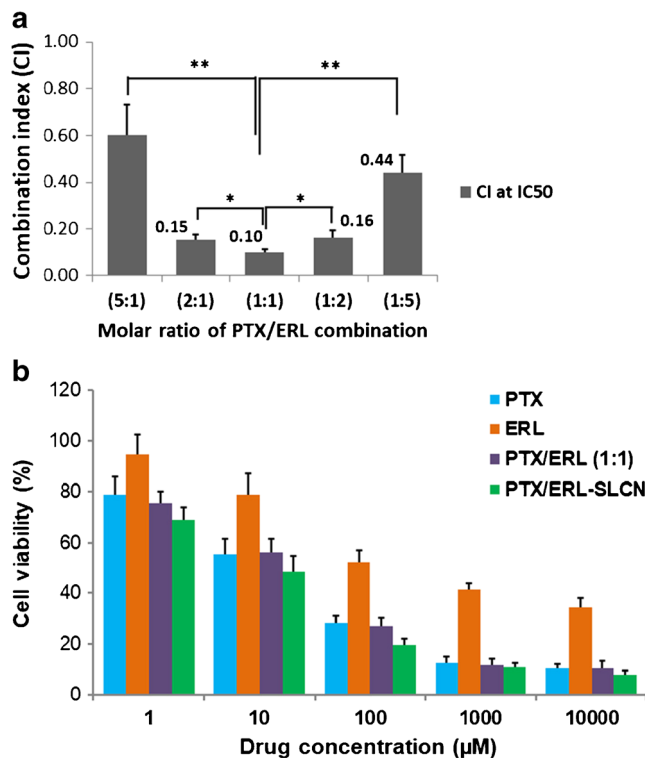
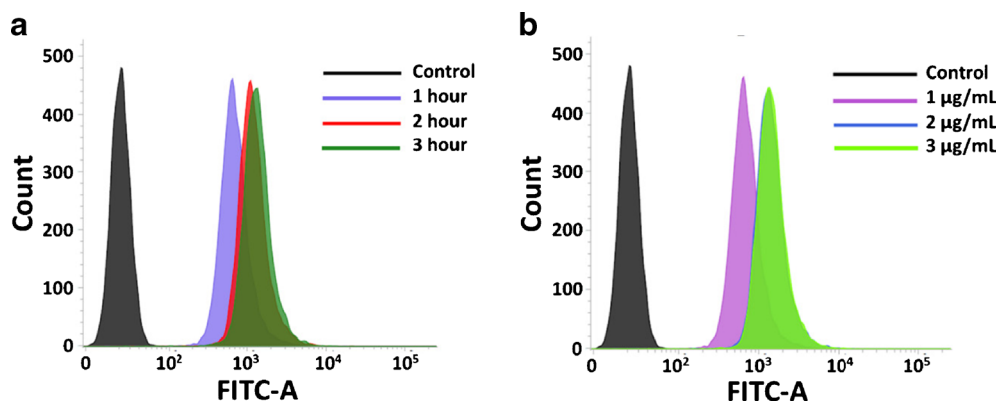


**Fig. 4** (a) Values of combination index (CI) at  $IC_{50}$  for various molar ratios of PTX/ERL combination in PTX/ERL-SLCN. The values have been represented as mean  $\pm$  SD. \*,  $p < 0.05$ ; \*\*,  $p < 0.01$ . (b) *In vitro* dose-dependent cytotoxicity of free PTX, free ERL, cocktail of free PTX and ERL (PTX/ERL, 1:1 w/w), and PTX and ERL co-loaded solid lipid core nanocapsules (PTX/ERL-SLCN) in NCI-H23 cell line.

**Fig. 5** Fluorescence-activated cell sorting (FACS) analysis to illustrate (a) time-dependent, and (b) concentration-dependent *in vitro* cellular uptake of coumarin 6-loaded solid lipid core nanocapsules (Cou-SLCN) in NCI-H23 cells



PTX and ERL was  $20.2 \pm 3.3\%$  and  $17.6 \pm 2.3\%$  at pH 7.4, and  $33.9 \pm 3.7\%$  and  $29.4 \pm 2.4\%$  at pH 5.0. This would effectively translate to relative stability of the system in circulation while showing enhanced drug release at the tumor site due to the relatively acidic pH in the tumor microenvironment (47). The disparity in release behavior based on pH of the release environment could be attributed to the protonation of the carboxyl moiety of the polyaspartate (mPEG-*b*-pAsp) in the nanoparticle corona specifically under acidic environmental conditions (44). Statistical evaluation of the drug release kinetics was

performed to explore and further elaborate the release mechanisms. The regression coefficients ( $r^2$  values) and the rate constants ( $K$ ) of the fitted release equations to various model equations are shown in Table S1. All four release equations showed best fit to Korsmeyer-Peppas model ( $r^2 > 0.9$ ), with release exponents ( $n$ ) of 0.81, 0.64, 0.89, and 0.74, respectively for release of PTX at pH 7.4 and pH 5.0 and of ERL at pH 7.4 and pH 5.0. This indicated non-Fickian or anomalous diffusion ( $n > 0.5$ ) that could be due to drug diffusion from the carrier as well as disintegration of the carrier itself (47,48).

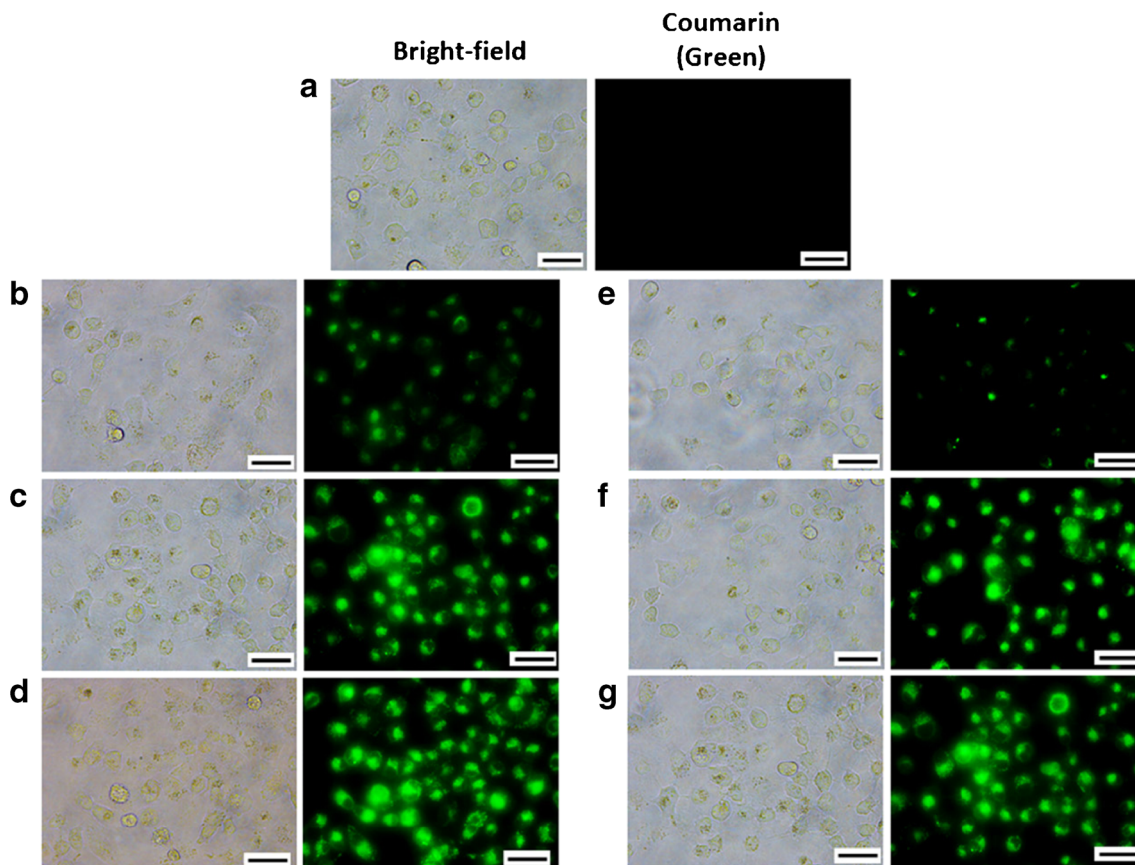


**Fig. 6** Fluorescence microscopic images showing time-dependent (b-d) and concentration-dependent (e-g) cellular uptake of coumarin 6-loaded solid lipid core nanocapsules (Cou-SLCN) in NCI-H23 cells. (a) Untreated control, (b) 1 h, (c) 2 h, (d) 3 h, (e) 1  $\mu\text{g/mL}$ , (f) 2  $\mu\text{g/mL}$ , (g) 3  $\mu\text{g/mL}$ . The scale bars = 50  $\mu\text{m}$ .

## Cytotoxicity Characteristics

Combination index (CI) analysis revealed that PTX/ERL-SLCN in all 5 M combinations of PTX and ERL (5:1, 2:1, 1:1, 1:2 and 1:5) resulted in synergic inhibition ( $CI < 0.9$ ) of the proliferation of NCI-H23 cell line (Fig. 4a). A PTX/ERL molar combination of 1:1 showed maximum synergism (minimum CI). Therefore, 1:1 was selected as the optimum molar combination ratio for PTX and ERL in PTX/ERL-SLCN, and all further PTX/ERL-SLCN formulations contained the drugs in the same ratio. MTT assay on NCI-H23 cells revealed dose-dependent cytotoxicity of PTX, ERL, PTX/ERL (1:1, molar ratio), and PTX/ERL-SLCN (Fig. 4b). The cytotoxic effect exerted by PTX/ERL-SLCN was markedly superior compared to those of PTX and ERL as well as PTX/ERL cocktail. To verify these cytotoxic effects,  $IC_{50}$  values for each treatment group were calculated by using standard equations (Table S2). The  $IC_{50}$  of PTX/ERL-SLCN was almost 3-fold lower than that of free PTX, and over 60-fold lower than that of free ERL. In contrast, while the  $IC_{50}$  of PTX/ERL cocktail was numerically similar to that of free PTX, it was over 20-fold lower than that of free ERL. Furthermore, the  $IC_{50}$  of PTX/ERL-SLCN was almost 3-fold lower than that of PTX/ERL cocktail.

## Cellular Uptake and Apoptosis

FACS analysis revealed excellent cellular uptake of Cou-SLCN by NCI-H23 cell line. The extent of cellular uptake appeared to progressively increase with time of incubation and with increasing concentration (Fig. 5). The excellent uptake of Cou-SLCN by NCI-H23 cell line was further confirmed by fluorescence microscopy, which showed similar time- and concentration-dependent uptake (Fig. 6). A dense green fluorescence, representing coumarin 6 loaded inside the SLCN carriers, in the cytosolic region of the NCI-H23 cells indicated that Cou-SLCN entered the cells, suggesting the SLCN carriers are capable of effectively delivering the synergistic combination of the cytotoxic drugs (PTX/ERL) specifically into the cancer cells. The mechanism which commonly regulates cellular uptake of particles below 200 nm is clathrin-mediated endocytosis (49). Therefore, clathrin-mediated endocytosis is considered to be the plausible mechanism of uptake of SLCN.

Early and late apoptosis of NCI-H23 cells in the control group and in response to 24-h treatment with PTX, ERL, PTX/ERL, and PTX/ERL-SLCN are shown in Fig. 7. The percentage of cells in early and late apoptosis phase after treatment with PTX/ERL-SLCN (51.3% and 20.5%,

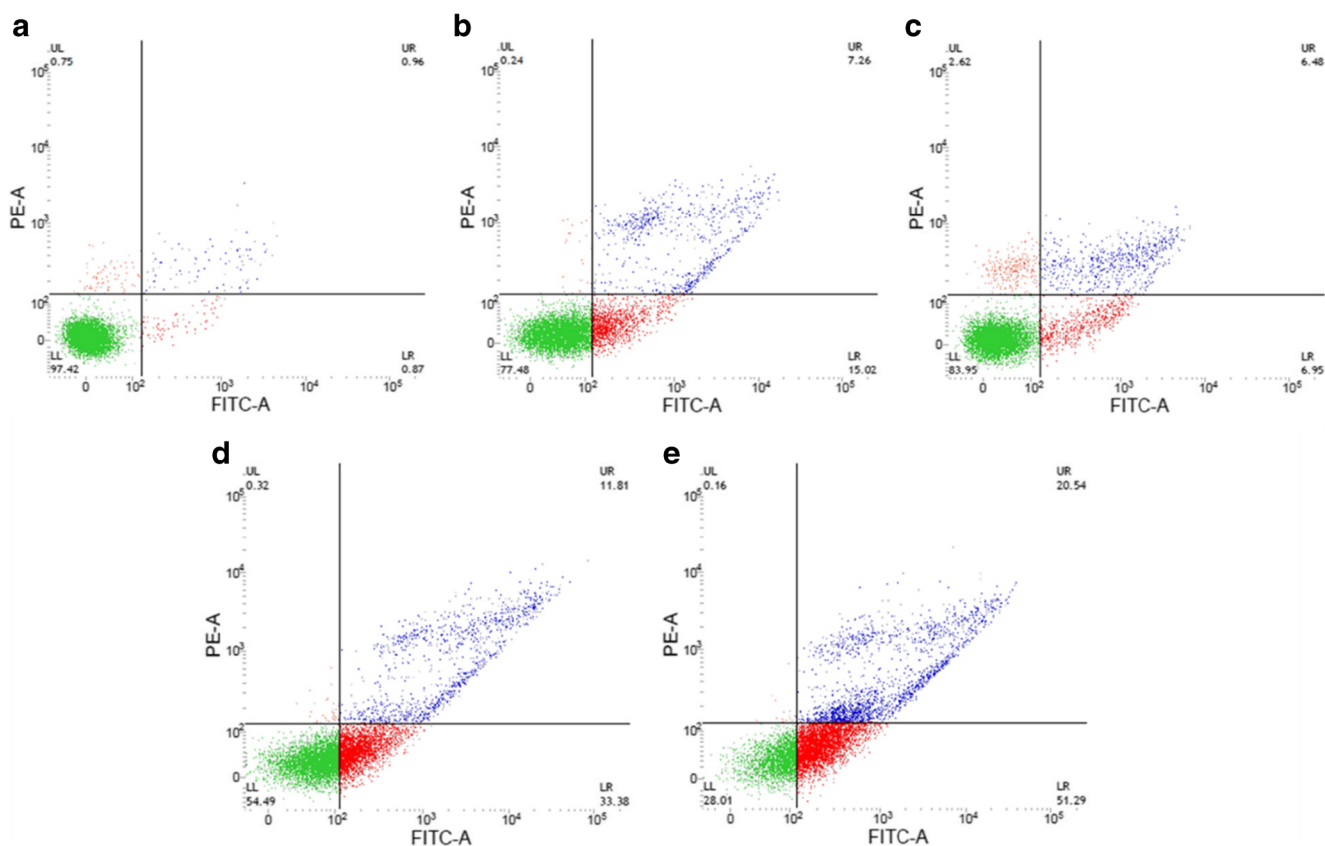


**Fig. 7** FACS analysis to demonstrate early and late apoptosis of NCI-H23 cells in (a) untreated control, (b) PTX, (c) ERL, (d) PTX/ERL, and (e) PTX/ERL-SLCN treated groups



respectively) was markedly higher than that not only after treatment with the individual free drugs (15.0% and 7.3% with PTX, and 6.9% and 6.5% with ERL) but also after treatment with the PTX/ERL cocktail (33.4% and 11.8%). These results corroborate with those of the cytotoxicity assay.

The apoptosis-related nuclear changes in NCI-H23 cells after treatment with PTX, ERL, PTX/ERL, and PTX/ERL-SLCN, as compared to the untreated control group, were observed by fluorescence microscopy following staining the nuclei with Hoechst 33,342 dye (Fig. 8). Nuclear fragmentation, a discernible sign of apoptosis, was clearly visible in all of the four treatment groups, including PTX, ERL, PTX/ERL, and PTX/ERL-SLCN. The degree of nuclear fragmentation observed in PTX/ERL-SLCN-treated cells was markedly higher than that in PTX, ERL, and PTX/ERL-treated cells, which was fully consistent with the results of the apoptosis assay.

## CONCLUSIONS

PTX/ERL-SLCN exhibited excellent physicochemical attributes, with nano-range particle size and high drug loading, along with pH-dependent and sustained release characteristics, all of which are highly suitable for drug delivery in cancer. It showed highly synergistic *in vitro* inhibition of NCI-H23 cell line, with remarkably lower  $IC_{50}$  than either of the free drugs. The cancer cells showed high uptake of the carrier and this was dependent on concentration and time of incubation. The formulation resulted in well-defined early and late apoptosis of the cancer cells with discernible signs of apoptosis-related changes in the nucleus, which were of higher magnitude than those resulting from the individual free drugs or the free drug cocktail. Therefore, we suggest that PTX/ERL-SLCN could be used as an optimal drug delivery carrier for effective chemotherapy of NSCLC.

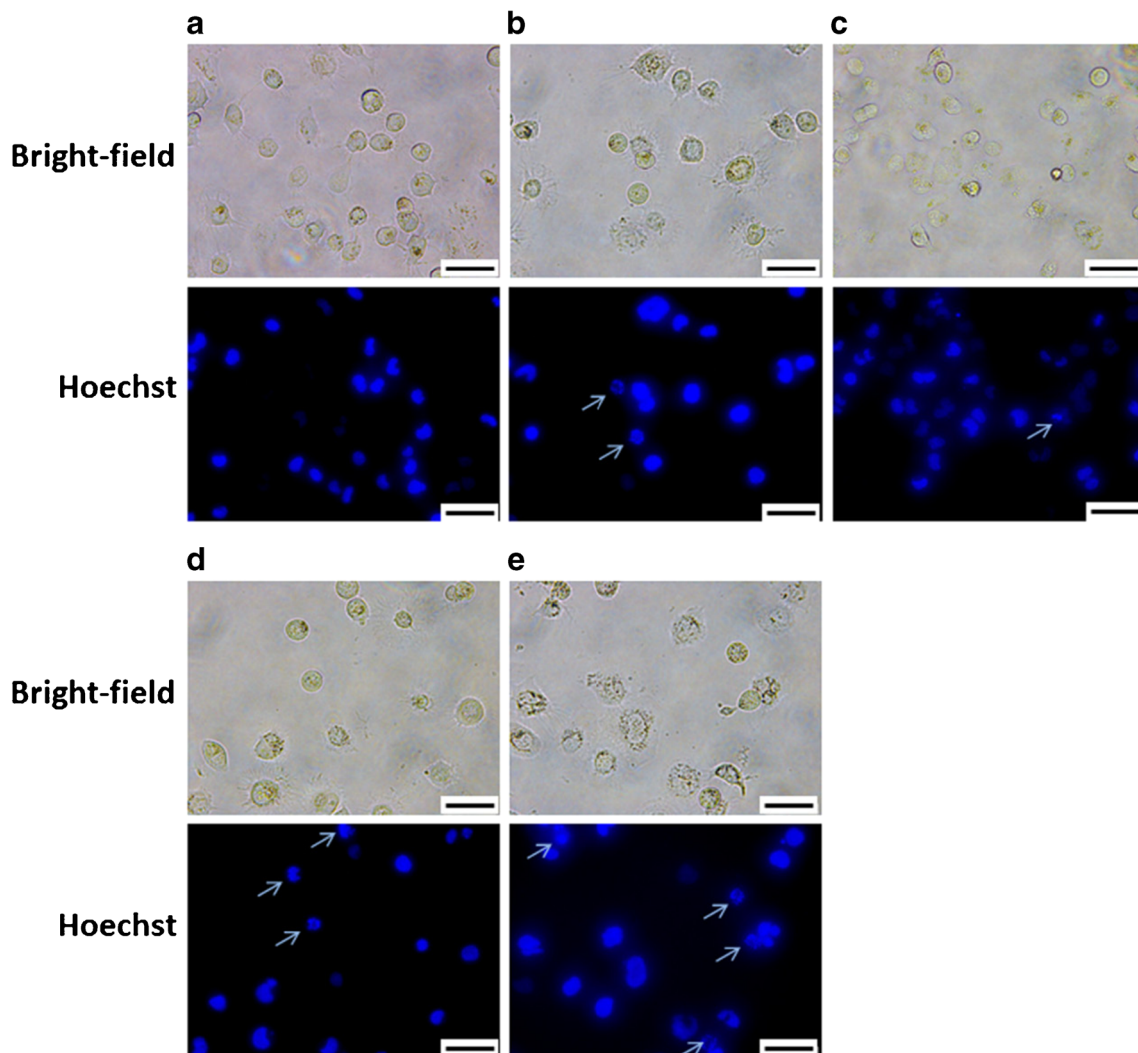


**Fig. 8** Hoechst staining to illustrate apoptosis-associated nuclear changes in (a) untreated control, (b) PTX, (c) ERL, (d) PTX/ERL, and (e) PTX/ERL-SLCN treated groups. The arrows indicate apoptotic nuclear fragmentation

## ACKNOWLEDGMENTS AND DISCLOSURES

This research was supported by the National Research Foundation of Korea (NRF) grant funded by the Korea government (MSIP) (No. 2015R1A2A2A01004118, 2015R1A2A2A04004806, and by the Medical Research Center Program (2015R1A5A2009124) through the NRF funded by MSIP).

## COMPLIANCE WITH ETHICAL STANDARDS

**Conflict of Interest** The authors have no conflict of interest to declare.

## REFERENCES

- Torre LA, Bray F, Siegel RL, Ferlay J, Lortet-Tieulent J, Jemal A. Global cancer statistics, 2012. *Ca-Cancer J Clin*. 2015;65:87–108.
- Molina JR, Yang P, Cassivi SD, Schild SE, Adjei AA. Non-small cell lung cancer: epidemiology, risk factors, treatment, and survivorship. *Mayo Clin Proc*. 2008;83(5):584–94.
- Zarogoulidis K, Zarogoulidis P, Darwiche K, Boutsikou E, Machairiotis N, Tsakiridis K, *et al*. Treatment of non-small cell lung cancer (NSCLC). *J Thorac Dis*. 2013;5(S4):S389–96.
- Cosaert J, Quoix E. Platinum drugs in the treatment of non-small cell lung cancer. *Br J Cancer*. 2002;87(8):825–33.
- Langer CJ, Manola J, Bernardo P, Kugler JW, Bonomi P, Cella D, *et al*. Cisplatin-based therapy for elderly patients with advanced non-small-cell lung cancer: implications of eastern cooperative oncology group 5592, a randomized trial. *J Natl Cancer Inst*. 2002;94(3):173–81.
- Rosell R, Crino L. Pemetrexed combination therapy in the treatment of non-small cell lung cancer. *Semin Oncol*. 2002;29:23–9.
- Cappuzzo F, Ciuleanu T, Stelmakh L, Cicenias S, Szczesna A, Juhasz E, *et al*. Erlotinib as maintenance treatment in advanced non-small-cell lung cancer: a multicenter, randomised, placebo-controlled phase 3 study. *Lancet Oncol*. 2010;11(6):521–9.
- Sandler A, Ettinger DS. Gemcitabine: single-agent and combination therapy in non-small cell lung cancer. *Oncologist*. 1999;4(3):241–51.
- Chen YM, Perng RP, Lee YC, Shih JF, Lee CS, Tsai CM, *et al*. Paclitaxel plus carboplatin, compared with paclitaxel plus gemcitabine, shows similar efficacy while more cost-effective: a randomized phase II study of combination chemotherapy against inoperable non-small cell lung cancer previously untreated. *Ann Oncol*. 2002;13(1):108–15.
- Freco FA. Paclitaxel-based combination chemotherapy in advanced non-small cell lung cancer. *Lung Cancer*. 2001;34:S53–6.
- Ramalingam S. First-line chemotherapy for advanced-stage non-small-cell lung cancer: focus on docetaxel. *Clin Lung Cancer*. 2005;7(Suppl 3):S77–82.
- Yang XQ, Li CY, MF X, Zhao H, Wang D. Comparison of first-line chemotherapy based on irinotecan or other drugs to treat non-small cell lung cancer in stage IIIB/IV: a systematic review and meta-analysis. *BMC Cancer*. 2015;15:949.
- Grunberg SM, Crowley JJ, Livingston RB, Muggia FM, MacDonald JS, Williamson SK, *et al*. Treatment of non-small-cell lung cancer with vinblastine and very high-dose cisplatin. A southwest oncology group study. *Cancer Chemother Pharmacol*. 1991;28(3):211–3.
- Faller BA, Pandit TN. Safety and efficacy of vinorelbine in the treatment of non-small cell lung cancer. *Clin Med Insights Oncol*. 2011;5:131–44.
- Monnet I, de Cremoux H, Soulie P, Saltiel-Voisin S, Bekradda M, Saltiel JC, *et al*. Oxaliplatin plus vinorelbine in advanced non-small-cell lung cancer: final results of a multicenter phase II study. *Ann Oncol*. 2002;13:103–7.
- Ardizzoni A, Antonelli G, Grossi F, Tixi L, Cafferata M, Rosso R. The combination of etoposide and cisplatin in non-small-cell lung cancer (NSCLC). *Ann Oncol*. 1999;10(suppl 5):S13–7.
- Sculier JP, Ghisdal L, Berghmans T, Branle F, Lafitte JJ, Vallot F, *et al*. The role of mitomycin in the treatment of non-small cell lung cancer: a systematic review with meta-analysis of the literature. *Br J Cancer*. 2001;84(9):1150–5.
- Hesketh PJ, Tansan S, Caquiao PB, Hesketh A, Blanchard R, DiMartino N, *et al*. Treatment of advanced non-small cell lung cancer with very high-dose cisplatin combined with etoposide and mitomycin C. *Cancer*. 1993;71(3):171–20.
- Cullen MH, Billingham IJ, Woodroffe CM, Chetiyawardana AD, Gower NH, Joshi R, *et al*. Mitomycin, ifosfamide, and cisplatin in unresectable non-small-cell lung cancer: effects on survival and quality of life. *J Clin Oncol*. 1999;17(10):3188–94.
- Babiak A, Hetzel J, Godde F, Konig HH, Pietsch M, Hetzel M, *et al*. Vinorelbine for second-line chemotherapy in NSCLC – a phase II trial. *Br J Cancer*. 2007;96:1052–6.
- Choi JY, Thapa RK, Yong CS, Kim JO. Nanoparticle-based combination drug delivery systems for synergistic cancer treatment. *J Pharm Invest*. 2016;46(4):325–39.
- Lilenbaum RC, Herndon JE, List MA, Desch C, Watson DM, Miller AA, *et al*. Single-agent versus combination chemotherapy in advanced non-small-cell lung cancer: the cancer and leukemia group B (study 9730). *J Clin Oncol*. 2005;23(1):190–6.
- Chen YM, Shih JF, Lee CS, Chen MC, Lin WC, Tsai CM, *et al*. Study of docetaxel and ifosfamide combination chemotherapy in non-small-cell lung cancer patients failing previous chemotherapy with or without paclitaxel. *Lung Cancer*. 2003;39(2):209–14.
- Sekine I, Saijo N. Novel combination chemotherapy in the treatment of non-small cell lung cancer. *Expert Opin Pharmacother*. 2000;1(6):1131–61.
- Tran TH, Thapa RK, Nguyen HT, Pham TT, Ramasamy T, Kim DS, *et al*. Combined phototherapy in anti-cancer treatment: therapeutics design and perspectives. *J Pharm Invest*. 2016;46(6):505–17.
- Lilenbaum R, Villalor VM, Langer C, O'Byrne K, O'Brien M, Ross HJ, *et al*. Single-agent versus combination chemotherapy in patients with advanced non-small cell lung cancer and a performance status of 2: prognostic factors and treatment selection based on two large randomized clinical trials. *J Thorac Oncol*. 2009;4(7):869–74.
- Santos FN, de Castria TB, Cruz MRS, Riera R. Chemotherapy for advances non-small cell lung cancer in the elderly population. (review) *Cochrane Database Syst Rev*. 2015; <https://doi.org/10.1002/14651858.CD010463.pub2>.
- Ramalingam S, Belani CP. Paclitaxel for non-small cell lung cancer. *Expert Opin Pharmacother*. 2004;5(8):1771–80.
- Chu Q, Vincent M, Logan D, Mackay JA, Evans WK. Taxanes as first-line therapy for advanced non-small cell lung cancer: a systematic review and practice guideline. *Lung Cancer*. 2005;50:355–74.
- Grindelli C, Bareschino MA, Schettino C, Rossi A, Maione P, Ciardiello F. Erlotinib in non-small cell lung cancer treatment: current status and future development. *Oncologist*. 2007;12:840–9.
- JL X, Jin B, Ren ZH, Lou YQ, Zhou ZR, Yang QZ, *et al*. Chemotherapy plus erlotinib versus chemotherapy alone for treating advanced non-small cell lung cancer: a meta-analysis. *PLoS One*. 2015; <https://doi.org/10.1371/journal.pone.0131278>.
- Leung L, Mok TSK, Loong H. Combining chemotherapy with epidermal growth factor receptor inhibition in advanced non-small cell lung cancer. *Ther Adv Med Oncol*. 2012;4(4):173–81.

33. Ma L, Kohli M, Smith A. Nanoparticles for combination drug therapy. *ACS Nano*. 2013;7(11):9518–25.
34. Hu CMJ, Aryal S, Zhang L. Nanoparticle-assisted combination therapies for effective cancer treatment. *Ther Del*. 2010;1(2):323–34.
35. Gupta B, Yong CS, Kim JO. Solid matrix-based lipid nanoplateforms as carriers for combinational therapeutics in cancer. *J Pharm Invest*. 2017;47(6):461–73.
36. Sharma A, Sharma US. Liposomes in drug delivery: progress and limitations. *Int J Pharm*. 1997;154:123–40.
37. Sercombe L, Veerati T, Moheimani F, SY W, Sood AK, Hua S. Advances and challenges of liposome assisted drug delivery. *Front Pharmacol*. 2015;6:Article 286.
38. Puri A, Loomis K, Smith B, Lee JH, Yavlovich A, Heldman E, *et al*. Lipid-based nanoparticles as pharmaceutical drug carriers: from concepts to clinic. *Crit Rev Ther Drug Carrier Syst*. 2009;26(6): 523–80.
39. Krishnamurthy S, Vaiyapuri R, Zhang L, Chan JM. Lipid-coated polymeric nanoparticles for cancer drug delivery. *Biomater Sci*. 2015;3:923–36.
40. Gupta B, Poudel BK, Pathak S, Tak JW, Lee HH, Jeong JH, *et al*. Effects of formulation variables on the particle size and drug encapsulation of imatinib-loaded solid lipid nanoparticles. *AAPS PharmSciTech*. 2016;17(3):652–62.
41. Varshosaz J, Ghaffari S, Khoshayand MR, Atyabi F, Azarmi S, Kobarfard F. Development and optimization of solid lipid nanoparticles of amikacin by central composite design. *J Liposome Res*. 2010;20(2):97–104.
42. Emami J, Mohiti H, Hamishehkar H, Varshosaz J. Formulation and optimization of solid lipid nanoparticle formulation for pulmonary delivery of budesonide using Taguchi and box-Behnken design. *Res Pharm Sci*. 2015;10(1):17–33.
43. Hao J, Fang X, Zhou Y, Wang J, Guo F, Li F, *et al*. Development and optimization of solid lipid nanoparticle formulation for ophthalmic delivery of chloramphenicol using a box-Behnken design. *Int J Nanomedicine*. 2011;6:683–92.
44. Gupta B, Pathak S, Poudel BK, Regmi S, Ruttala HB, Gautam M, *et al*. Folate receptor-targeted hybrid lipid-core nanocapsules for sequential delivery of doxorubicin and tanespimycin. *Colloids Surf B: Biointerfaces*. 2017;155:83–92.
45. Kobayashi H, Watanabe R, Choyke PL. Improving conventional enhanced permeability and retention (EPR) effects; what is the appropriate target? *Theranostics*. 2014;4(1):81–9.
46. Gupta B, Poudel BK, Tran TH, Pradhan R, Cho HJ, Jeong JH, *et al*. Modulation of pharmacokinetic and cytotoxicity profile of imatinib base by employing optimized nanostructured lipid carriers. *Pharm Res*. 2015;32(9):2912–27.
47. Gupta B, Ramasamy T, Poudel BK, Pathak S, Regmi S, Choi JY, *et al*. Development of bioactive PEGylated nanostructured platforms for sequential delivery of doxorubicin and imatinib to overcome drug resistance in metastatic tumors. *ACS Appl Mater Interfaces*. 2017;9:9280–90.
48. Korsmeyer RW, Gurny R, Doelker E, Buri P, Peppas NA. Mechanisms of solute release from porous hydrophilic polymers. *Int J Pharm*. 1983;15:25–35.
49. Rejman J, Oberle V, Zuhorn IS, Hoekstra D. Size-dependent internalization of particles via the pathways of clathrin- and caveolae-mediated endocytosis. *Biochem J*. 2004;377(1):159–69.